

Two Design Procedures for PM Synchronous Machines for Electric Powertrains

*Original*

Two Design Procedures for PM Synchronous Machines for Electric Powertrains / Lu, Chao; Ferrari, Simone; Pellegrino, GIAN - MARIO LUIGI. - In: IEEE TRANSACTIONS ON TRANSPORTATION ELECTRIFICATION. - ISSN 2332-7782. - 3:1(2017), pp. 98-107. [10.1109/TTE.2016.2646738]

*Availability:*

This version is available at: 11583/2664444 since: 2017-07-06T11:25:47Z

*Publisher:*

IEEE

*Published*

DOI:10.1109/TTE.2016.2646738

*Terms of use:*

This article is made available under terms and conditions as specified in the corresponding bibliographic description in the repository

*Publisher copyright*

(Article begins on next page)

# Two Design Procedures for PM Synchronous Machines for Electric Powertrains

Chao Lu, Simone Ferrari and Gianmario Pellegrino, *Senior Member, IEEE*  
Department of Energy, Politecnico di Torino, 10129 Turin, Italy

**Abstract**—This paper presents a design environment for permanent-magnet synchronous motors (PMSMs). Two design examples for electric vehicle (EV) traction are presented: one interior PM machine of the PM-assisted synchronous reluctance (PM-SyR) type and one concentrated-winding surface-mounted PM motor (CW-SPM). The parametric design software used in the paper includes design equations, finite element analysis (FEA) and multi-objective optimization algorithms for the design of PMSMs. The paper presents two possible design methodologies, for the two mentioned test cases. EV application was chosen for its many challenging aspects, involving flux weakening for extended speed range, discontinuous duty cycles, high transient overload requirements, high efficiency over a large area of operation, and so forth. The design examples are compared to selected benchmark designs in terms of operating range in the torque versus speed domain and efficiency maps, all FEA evaluated. Besides magnetics, thermal and structural aspects are included in the study.

**Index Terms**— Automatic design, Parametric design, Electrical Machine Design, Finite element analysis, Permanent-magnet motor, Traction motor drives.

## I. INTRODUCTION

Electrical machines design is a complex, multi-objective engineering challenge whose typical goals are maximizing the output torque, minimizing losses, mass, cost, torque ripple, etc... Magnetic aspects play the central role in the design, but many other non-secondary aspects make this a multi-physical problem and a kaleidoscopic challenge. Recent efficiency standards [1] demand for accurate loss evaluation and thermal-magnetic co-design. Today's demanding applications like the more electric aircraft [2] or vehicle powertrains [3-5] ask for high compactness, transient operation in a variety of operating points, and high efficiency in all operating conditions. A number of non-magnetic aspects must be taken into account, such as structural co-design for high-speed operation [6-7], sustainable iron and permanent magnet (PM) losses [8], flux weakening capability, transient overload capability, and high efficiency in a large operating region [9], as said. The multi-objective design problem is thus becoming complicated more and more. Fortunately, the growing complexity of application requirements is backed by an even stronger growth of artificial intelligence and available computational resources. This study illustrates two different design procedures for PM synchronous machines (PMSMs), integrated in a machine design environment SyR-e [10], linked with finite element analysis (FEA) engine FEMM [11]. Two exemplar design approaches are presented, for PMSMs of two different types.

The traction motor of an electric vehicle (EV) is one of the most challenging application design wise. Its mission contains

a multitude of transient operating points, defined by the different possible driving cycles of the vehicle. The PMSMs applied to EVs are the concentrated-winding surfaced-mounted PM (CW-SPM) machine and the interior PM (IPM) machine. PM-assisted Synchronous Reluctance (PM-SyR) motors are a subclass of IPM machines appreciated in EV traction for their good efficiency properties and for the possibility of using ferrite magnet in place of rare-earth magnet [12]. Previous work compared CW-SPM and PM-SyR machines to the Induction Machine (IM) in EV application [13]. This paper uses the traction motors presented in [13] as the benchmark for two new designs made in SyR-e. The two types of machines considered here are the CW-SPM and the PM-SyR ones. The latter is designed through a parametric model based on design equations [14-15], and FEA simulated at a later stage for the sake of accurate performance evaluation. Conversely, the CW-SPM machine is designed using an automatized approach, based on multi-objective differential evolution (MODE) and FEA [16-17]. After the design part, both machines are FEA characterized in detail, including the study of iron and PM losses, the determination of the control trajectories like the maximum torque per ampere (MTPA) law and the flux-weakening law. The limits of the torque – speed envelope given the power converter will be put in evidence, alongside calculated efficiency maps, as final performance indicators against the reference machines of [13]. All operations presented in the paper can be repeated by the reader using online resources of SyR-e, with the only exception of iron and PM loss evaluation, for now delegated to commercial software [18]. The main contributions of the paper are: 1) to provide comprehensive design procedures for PM-SyR and CW-SPM machines for traction, where most of key aspects are taken into account. 2) Such design strategies take advantage of shortcuts purposely intended for traction motors, such as the goal function  $\lambda_{d,180^\circ}$  that summarizes flux weakening capability in one FEA simulation. 3) The consequence of 2) is that no extensive optimization covering multiple operating points in the torque versus speed plane was required to obtain satisfactory performance and high efficiency. 4) To present the concept of PM-assistance using the fictitious magnet and the magnet substitution principles. 5) To provide most of the tools needed for reproducing the results presented in the paper.

## II. DESIGN ENVIRONMENT

SyR-e stands for Synchronous Reluctance evolution and it is based on the interaction between Matlab (or Octave) and the 2D magnetic FEA client FEMM. This was made possible by the Octave-FEMM scripting library [11]. The basic principle of operation of SyR-e is depicted in Fig. 1. SyR and PM-SyR

machines are covered. SPM rotors are also selectable, as well as CW configurations, for all rotor types, via a graphical user interface (GUI).

The simpler operation that SyR-e can do is parametric FEA simulation and manipulation of the results. The user can define the design through the GUI and then run FEA simulations in FEMM to obtain torque and flux maps, for example. Simulations results can be further processed in Matlab, to obtain control trajectories including maximum torque per ampere and per volt (MTPA, MTPV) laws, flux weakening laws, and efficiency maps. Eventually, the design can be exported to other CADs for other types of evaluation.

A second possible approach is to use the design equations integrated into SyR-e. The user can design the machine using the design equations in a parametric fashion, pick up a design from the plane of the parameters, and then verify its performance in FEMM. Design optimization is also included. A large set of geometric and non-geometric parameters can be optimized using MODE, using FEMM for fitness evaluation. Finally, non-magnetics aspects are covered, namely preliminary thermal and structural analyses, as addressed in Section VI.

### III. DESIGN SPECIFICATIONS

#### A. Reference Data

This study uses the same volume constraints and power converter ratings previous work [13]. The ratings of benchmark motors and new designed motors are reported in Table I. The objective of this study is to illustrate the design methodology and possibly obtain machines with a higher power versus speed envelope and with lower loss in key operating areas.

TABLE I - REFERENCE DATA

		PM-SyR		CW-SPM	
		[13]	present	[13]	present
Converter phase voltage	V pk	173			
Converter current	A pk	360			
Stack length	mm	170			
Steel grade		M250-35A			
PM grade		BMN-42SH			
Copper temperature	°C	150			
Rotor temperature	°C	130			
Pole pairs		2			
Rated current	A	≥ 192 A			
Torque at base speed	Nm	120			
Base speed $\omega_{base}$	rpm	about 4,000			
Power target at max. speed	W	50,000 (point F)			
Max speed $\omega_{max}$	rpm	12,000			
Stator outer diameter	mm	216			
Number of slots		48		6	
Stator bore diameter	mm	142	124	128	
Airgap	mm	0.7	0.7	1	
Copper fill factor		0.4	0.4	0.55	
Number of turns		20	24	23	24
Torque @ 360 A	Nm	210	240	150	164
Characteristic current	A pk	205	204	193	198
Phase resistance @ 130°C	Ω	0.027	0.023	0.026	0.02
Magnet Mass	kg	1.95	1.24	1.35	2.17

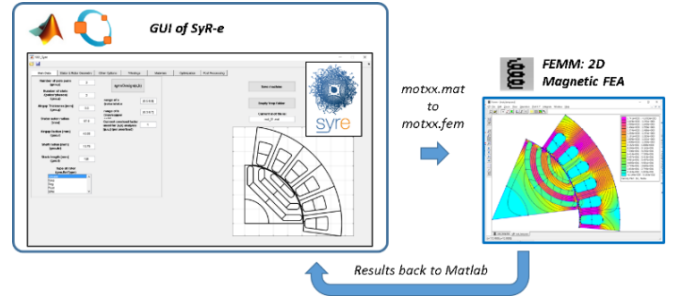


Fig. 1. Principle of operation of SyR-e

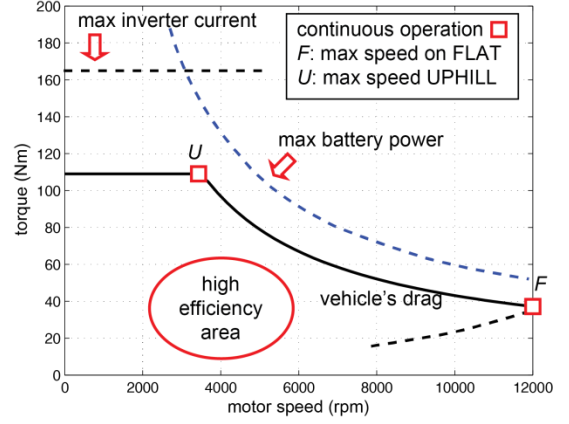


Fig. 2. Torque versus speed requirements of an electric vehicle

#### B. Key Design Conditions for EV Application

When dealing with a vehicle powertrain, it is not easy to extract a single operating condition as the only reference for magnetic and thermal design. The typical torque versus speed envelope of an EV traction drive is reported in Fig. 2. It has a large constant power speed range, dictated by the power converter and battery limits. Besides maximizing torque at low speed, the designer must fulfill the power target at maximum speed, in flux weakening operation. Two key design points summarize the magnetic design:

- 1) Point U (110 Nm, 4,000 rpm, stands for up-hill) in Fig. 2 represents worst case climbing conditions.
- 2) Point F (39 kW, 12,000 rpm, stands for flat) represents the power required to run the vehicle at its maximum speed.

Both design conditions refer to quasi-continuous operation, intending that both situations can be prolonged in time for more than one thermal time constant, even if this is not strictly specified by driving cycle used for this vehicle (NEDC: new European driving cycle [19]). Point U defines the rated torque, whereas point F defines the flux weakening speed range of the drive.

#### C. Single Operating Point Design

The steady state model of a PMSM is briefly reviewed:

$$v_{dq} = R_s i_{dq} + j\omega \lambda_{dq} \quad (1)$$

$$\lambda_{dq} = \begin{bmatrix} L_d & 0 \\ 0 & L_q \end{bmatrix} \cdot i_{dq} + \begin{bmatrix} \lambda_m \\ 0 \end{bmatrix} \quad (2)$$

Where  $v_{dq}$ ,  $i_{dq}$  and  $\lambda_{dq}$  respectively are the voltage, current and flux linkage vectors in rotor coordinates  $dq$ ,  $R_s$  is the

phase resistance,  $\omega$  is the rotor speed in electrical degree [rad/s],  $L_d$  and  $L_q$  are inductance in  $d$  and  $q$  axes,  $\lambda_m$  is PM flux linkage, The electromagnetic torque (3) has one magnet component (term with  $\lambda_m$ ) and one reluctance (term with  $L_d - L_q$ ) component.

$$T = \frac{3}{2}p \cdot [\lambda_m i_q + (L_d - L_q) \cdot i_d i_q] \quad (3)$$

Where  $p$  is number of pole pairs. The PM-SyR and the CW-SPM motors have different combinations of magnet and reluctance torque. The former exploits reluctance torque as much as possible, whereas the latter has  $L_d \cong L_q$  thereby only magnet torque.

**Target torque is defined after point U. Point F dictates that flux weakening capability is sufficient. It means that the motor is able to reach the required power at maximum speed under maximum voltage constraint.** A powerful metric of flux weakening capability of a PMSM is its characteristic current:

$$i_{ch} = \frac{\lambda_m}{L_d} \quad (4)$$

At current level (4), the armature flux can cancel the magnet flux, if the current vector is aligned against the magnet direction. Fig. 3 reports the vector diagram of one PM-SyR and one CW-SPM machines operating at their characteristic current. Starting from the respective MTPA conditions, i.e. from full torque and full flux, flux weakening is applied via rotation of the current vector (dashed trajectories), eventually ending into zero flux conditions (red circle in Fig. 3). Neglecting losses, the power versus speed curve of both such PMSMs is asymptotically flat (Fig. 4), with a plateau called the characteristic power:

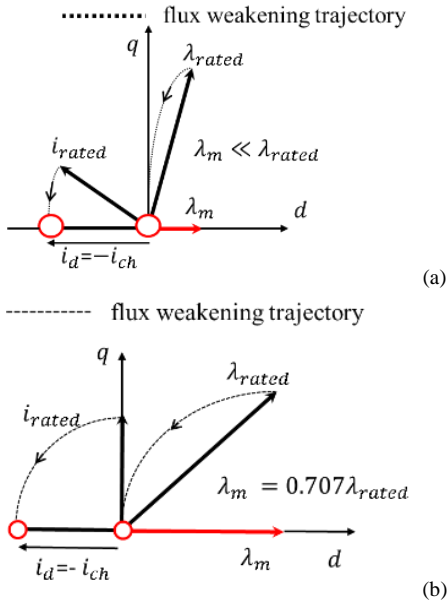


Fig. 3. Vector diagram of two PMSMs supplied at their characteristic current, a) PM-SyR; b) CW-SPM

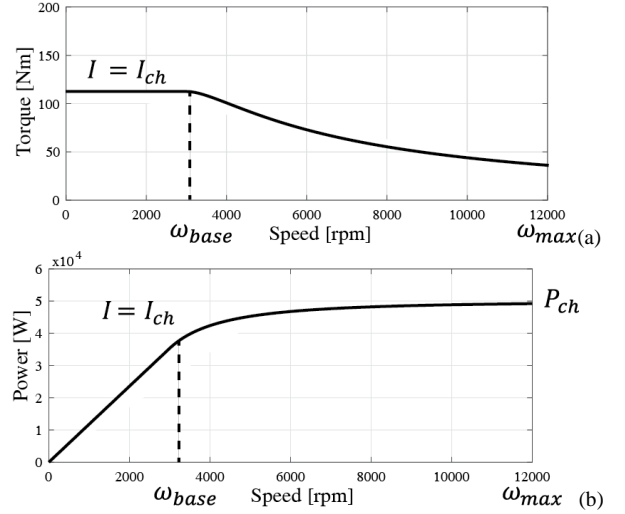


Fig. 4. Torque (a) and power (b) versus speed profiles of two PMSMs supplied with their characteristic current, under constrained voltage.

$$P_{ch} = \frac{3}{2} \cdot V_{max} \cdot i_{ch} \quad (5)$$

This paper considers machines **1) having the characteristic power equal to rated power at maximum speed**, and **2) enough torque at low speed to fulfill design condition U**. To do so, the two design conditions U and F will be merged into a single optimization, with different methodologies for the two designs.

#### IV. PM-SyR MACHINE DESIGN

##### A. Three-Step Design Procedure

The design of the PM-SyR machine uses design equation and FEA together. This is an example of design procedure without use of optimization algorithms. The design procedure starts with the design of an appropriate SyRM (SyRM). This should have adequate torque and power factor (PF). Torque of the SyRM will be reflected into torque of the final PM-SyRM design: the initial SyRM normally targets 70-80% of the final PM-SyRM torque<sup>1</sup>. At the same time, the better the PF of the SyRM, the smaller the magnet quantity needed in the final PM-SyRM design, for the same output power at high speed.

After the SyRM design, flux barriers are filled with fictitious magnets having remanence  $B_r'$ , and this is FEA calibrated to reach the desired characteristic power. Eventually, the fictitious magnet is replaced with a magnet of higher strength and smaller volume, via a simple scaling rule. The three design steps are illustrated in the flowchart reported in Fig. 5.

##### B. Key Constraints and Inputs

With reference to Fig. 5, outer dimensions of the stack ( $D$

<sup>1</sup> Typical values of torque split ratio between the initial SyRM and the final PM assisted version come from power factor considerations: a good SyRM has a PF of 0.70 – 0.75 at nominal torque. PM assistance leads the PF in the neighborhoods of 1.0. The PF improvement reflects into an improvement of nominal torque of the same amount. For example initial PF equal to 0.70, final PF equal 1.0: this means the torque of the SyRM is 70% of the one of the PM-SyRM. If the initial PF is 0.7 and the final PF is <1.0, e.g. 0.87, then the torque ratio is 80%.

and  $L$ ) are fixed from the very beginning, according to space constraints. Another key initial input is the thermal loading, expressed in the form of copper loss per outer stack surface  $k_j$  [ $\text{W}/\text{m}^2$ ].

$$k_j = \frac{\text{Copper loss}}{\pi DL} = \frac{(6N_s I)^2}{\rho \frac{k_{Cu} L}{L_{end} + L} 2\pi D \cdot A_{Slots}} \quad (6)$$

The thermal loading factor has to do with total peak Ampere-turns ( $6N_s I$ , where  $N_s$  is the number of turns in series per phase), physical size ( $D, L$ ) and windings properties ( $A_{Slots}$ : total slots area,  $k_{Cu}$ : copper filling factor,  $\rho$ : copper resistivity,  $L_{end}$ : length of end turns). After the size and windings are defined, the thermal loading (6) is indirectly defining the admitted level of electrical loading of the machine. Using (6) in place of the electrical loading provides an insightful link to the heat extraction capability of the considered cooling setup. Here a value of  $k_j = 11,000$  [ $\text{W}/\text{m}^2$ ] is considered, based on past designs experience and commercial motors used on traction application [20]. Then thermal estimation and validation are applied to verify the selection of thermal loading. Thermal verification is not represented in the flowchart, and will be discussed later.

Structural constraints related to maximum operating speed are included in the design pipeline with simplified equations and off-line verified with FEA at the end of the design process. This is discussed in Section VI.

### C. Torque – Power Factor Plane

Step one of the design procedure (torque – PF tradeoff of the SyRM) uses parametric design equations in the  $(x, b)$  plane. The design parameters  $x$  and  $b$  are the rotor/stator diameters ratio (7) and the normalized airgap flux density (8),

respectively, and this approach comes from [12-13]:

$$x = r/R \quad (7)$$

$$b = \frac{B_g}{B_{Fe}} \quad (8)$$

$r$  in (7) is the rotor radius,  $R = D/2$  is the stator outer radius,  $B_g$  is the peak flux density at the airgap and  $B_{Fe}$  is the peak flux density in the iron (teeth, yoke and rotor flux barriers). Most of stator and rotor geometrical quantities all depend on  $x$  and  $b$ , as suggested in Fig. 6a. The factor  $b$  represents the per unit steel quantity, because it determines the cross section of the iron elements.

The tradeoff between torque and power factor is established from the  $(x, b)$  plane (Fig. 7). Each point of the plane represents one design. Four design examples taken from the plane are reported alongside the parametric plane. As  $x$  grows ( $a$  to  $b$  or  $c$  to  $d$ ), the rotor becomes bigger and stator slots become shorter. On the other hand, when  $b$  grows ( $c$  to  $a$ , or  $d$  to  $b$ ) stator and rotor steel elements get thicker, at the cost of reduced stator slot and rotor barrier areas. Design (c) is the one selected here. If necessary (torque not sufficient, or too high), the initial inputs should be changed and the process is repeated.

### D. Magnet Design

The barriers are filled with fictitious magnet material having remanence  $B_r'$  that can vary with continuity starting from 0 Tesla. Given the SyRM geometry and the input  $k_j$ , the  $B_r'$  parameter determines the characteristic power of the machine at constrained voltage (5) [21]. The effect of  $B_r'$  on the power – speed curve of the considered PM-SyRM is reported in Fig. 8. The final correct value of  $B_r'$  here is found to be  $B_r' = 0.44$  T, corresponding to the target characteristic

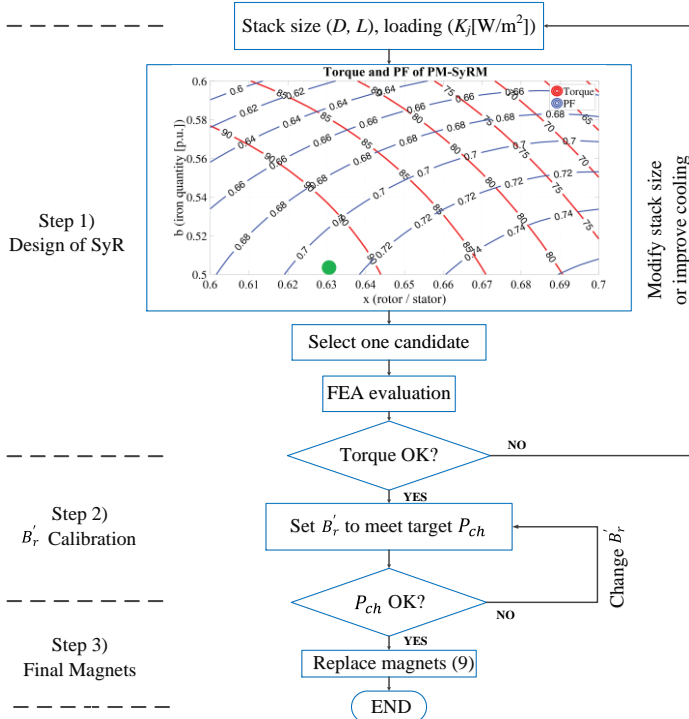


Fig. 5. Design Flowchart used for the PM-SyRM

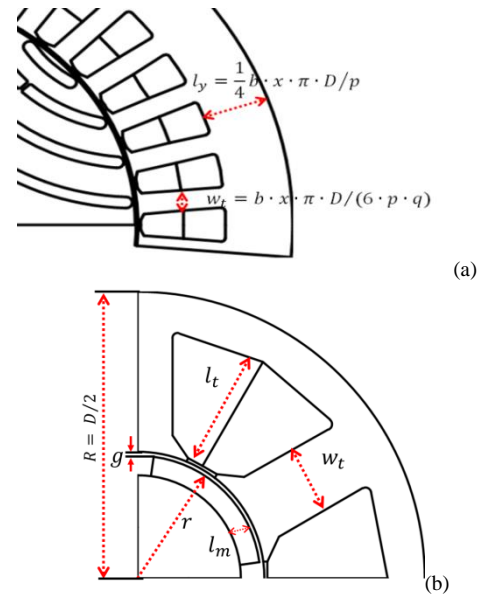


Fig. 6. Definition of parametric of machine geometry, a) PM-SyR; b) CW-SPM

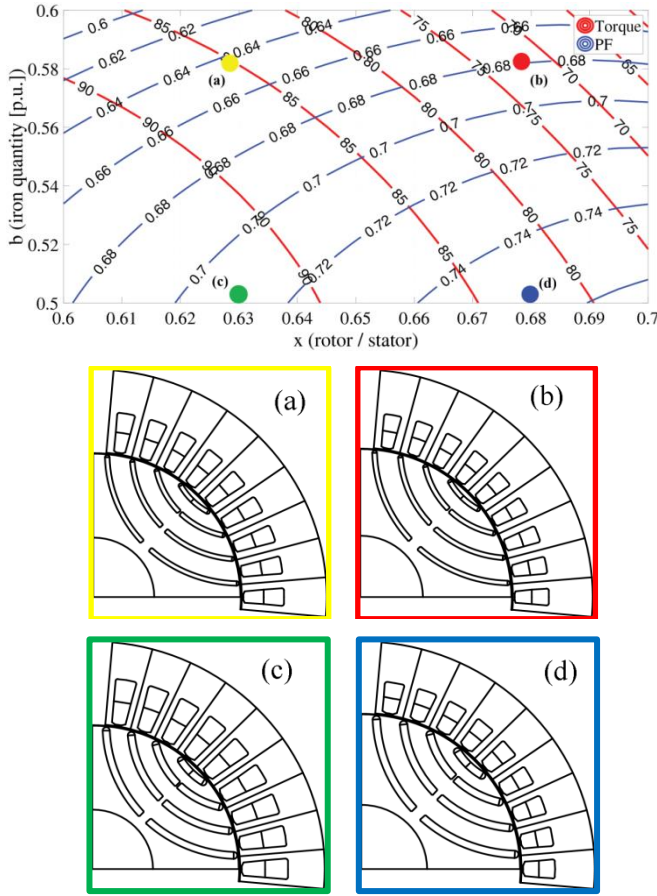


Fig. 7. Parametric design plane of the initial SyRM, for torque and Power Factor tradeoff and four design examples

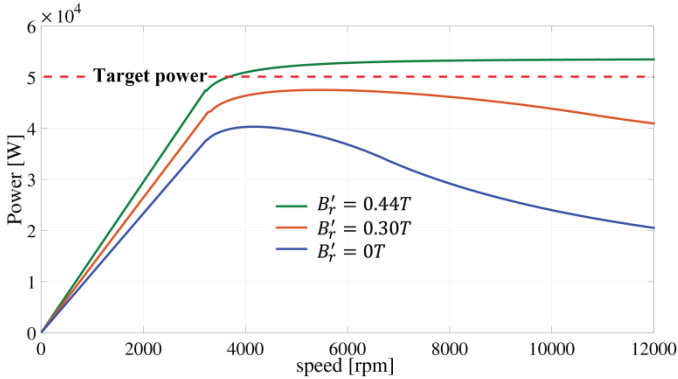


Fig. 8. Effect of the design parameter  $B_r'$  on the power versus speed curve at 204 A,  $V_{dc} = 300V$

power of 50 kW (Fig. 8). The fictitious magnets approach permits to fine-tune the characteristic power condition, with a limited number of FEA simulations.

### E. Final Magnet Design

Finally, the fictitious magnet is substituted with a smaller volume of commercial magnet, having remanence equal to  $B_r$ . PM volumes ( $V_m$ ) and remanence are in inverse proportions.

$$\frac{V_m}{V_m'} = \frac{B_r'}{B_r} \quad (9)$$

The relationship (9) is applied to each rotor barrier, individually. It is obtained via the magnetic circuit model of

one barrier, and imposing that the flux crossing the barrier at zero current conditions is the same either when excited by a magnet of remanence  $B_r'$  and volume  $V_m'$  equal to the barrier's volume, or by a smaller magnet ( $V_m < V_m'$ ) having higher remanence  $B_r$ . The average torque and maximum power performance are not affected by the magnet substitution. For example, the fictitious PM with  $B_r' = 0.44 T$  is replaced here with grade BMN-42SH, having  $B_r = 1.09 T$  at  $150^\circ C$ . The performance of the machine before and after magnet substitution is summarized in Table II. The parametric design is carried out in piecewise ideal conditions, i.e. linear iron, airgap ribs saturated, so it is possible to see some differences between the performances estimated in the  $(x, b)$  plane and the FEA results.

For better clarity, the field distributions of the two machines at open circuit conditions are reported in Fig. 9. The magnetization direction of PMs is towards to the arc center of the flux barriers. Although the field lines and flux density values in the two rotors are different from each other, the filed lines in the stator are exactly the same for the two machines. This suggests the effectiveness of the substitution, confirmed by Table II. Local saturation in the rotor is more intense when the stronger magnet is adopted, but this has little effect on the performance “at the terminals”. PM flux leakage through the structural ribs is the same with both magnet types: the bridges are fully saturated already from zero stator current conditions.

### F. Comprehensive Performance Evaluation

After the design stage is completed, the candidate machine is FEA evaluated comprehensively in terms of flux maps, iron and PM loss maps and the manipulation of the above. FEA maps are off-line processed to obtain key control laws and, finally, the efficiency map in the torque – speed plane. Relevant results are reported in Section VII. Structural and thermal issues are partly covered by SyR-e and partly verified off-line, as described in section VI.

## V. DESIGN OF THE CW-SPM WITH THE MODE

Parametric analysis in the  $(b, x)$  plane is possible also for the SPM machine. For the sake of showing a different approach, the CW-SPM machine was designed by means of multi-objective optimization. Optimization goals are torque and flux weakening capability.

### A. Design Flowchart

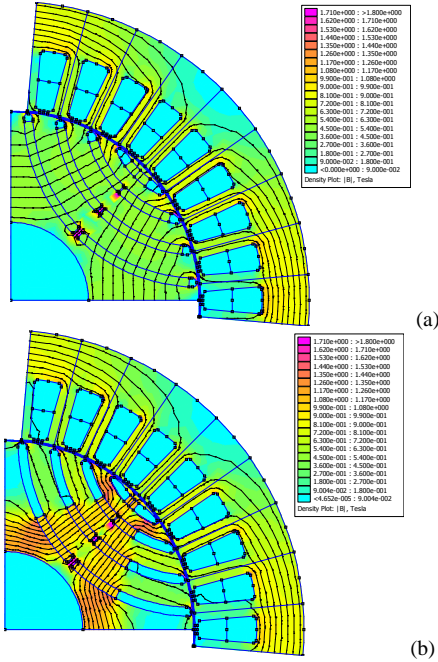
The design flowchart is reported in Fig. 10, for the CW-SPM machine. As for the PM-SyR case,  $D$  and  $L$  [m] are the initial inputs, along with  $k_j$  ( $11,000 W/m^2$ ). Another key input is the airgap thickness  $g$ , coming from mechanical constraints. The optimization inputs are tooth length  $l_t$  and width  $w_t$ , magnet thickness  $l_m$ , and rotor outer radius  $r$ , defined in Fig. 6b. The MODE optimization algorithm produces a Pareto front in two dimensions. One solution machine is selected from the Pareto front (green marker), as explained in the following.

### B. Two-Goal MODE Optimization

The first design goal is torque, evaluated with a current phase angle  $\gamma = 90^\circ$ , corresponding to MTPA production, as

TABLE II PM-SYRM DESIGN SUMMARY

	Baseline SyRM		PM-SyRM	
	Estimated	FEA	Fict. PMs ( $B_r'$ )	BMN-42SH ( $B_r$ )
Remanence [T]	/	/	0.44	1.09
PM volume [liters]	0	0	0.122	0.049
Load conditions: 204 A ( $k_f = 11,000 \text{ W/m}^2$ )				
Torque [Nm]	92	88	130	131
PF	0.71	0.60	0.86	0.87
$P_{ch}$ [kW]	/	/	53,410	53,440
Open circuit conditions (@ 4,000 rpm)				
Line back-emf [V] pk	0	0	37.7	38.5
Iron Loss @ 12,000 rpm, open circuit				
Stator	/	/	301	342
Rotor	/	/	70	78


 Fig. 9. FEA evaluated field distributions for the PM-SyRM design at zero current conditions. a) Fictitious PMs ( $B_r' = 0.44 \text{ T}$ ); b) Final PMs ( $B_r = 1.09 \text{ T}$ )

reported in Fig. 11a. The second design goal is the metric of the flux weakening capability of the machine and it is called  $\lambda_{d,180^\circ}$ . The goal function  $\lambda_{d,180^\circ}$  accounts for the  $d$ -axis flux linkage when the current vector is aligned against the PMs ( $\gamma = 180^\circ$ , Fig. 11b). If this is positive, then the characteristic current of the candidate design is larger than the simulated current. The opposite is true for negative values of  $\lambda_{d,180^\circ}$ . If this is zero, then the candidate design is exactly in characteristic current conditions. Fig. 11 describes how the two goals are FEA evaluated during the optimization process. Torque evaluation (Fig. 11a) requires the simulation of at least 5 rotor positions over one stator slot pitch to account for torque ripple effect. The first position is randomly selected

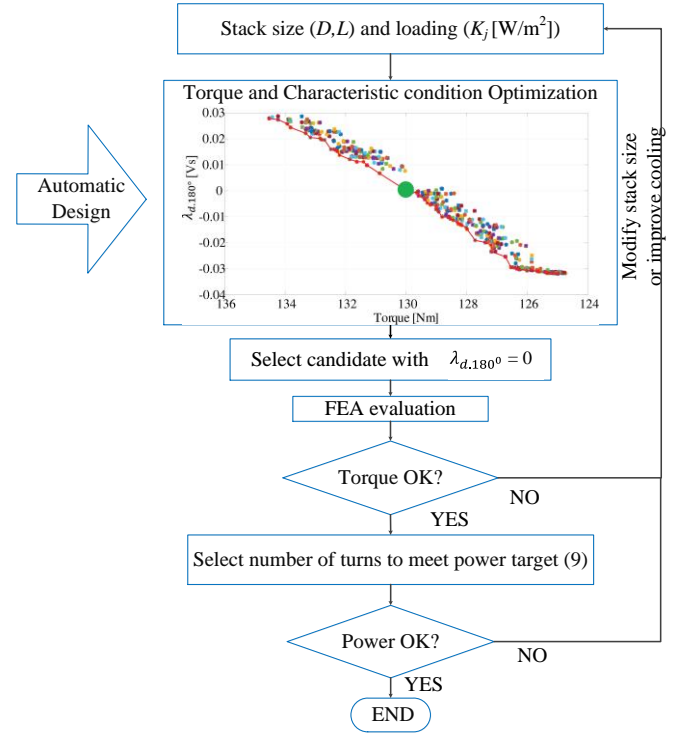
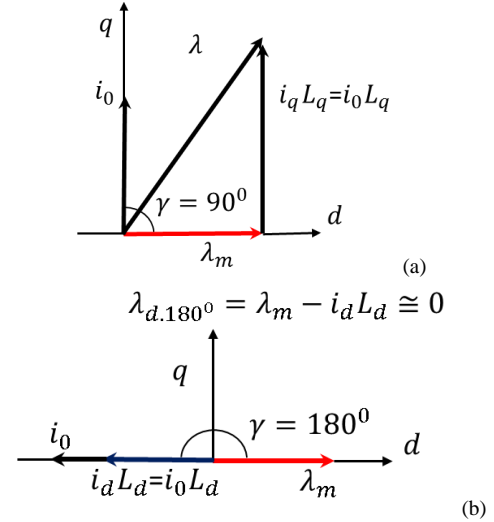


Fig. 10. Design Flowchart used for the CW-SPM


 Fig. 11. a) Torque evaluation, current is placed at  $\gamma = 90^\circ$ . b) Flux weakening capability evaluation: current is placed at  $\gamma = 180^\circ$ 

within one fifth of the stator slot pitch, and then other four positions are distributed evenly [21]. One additional simulation is used to evaluate the residual flux linkage  $\lambda_{d,180^\circ}$  (Fig.11b). All included, this makes 6 static FEA simulations per candidate. The anticipated Pareto front required the evaluation of 10,000 individuals, for a total 60,000 FEA simulations. This took 26.5 hours on a standard desktop computer (Intel Core i7-2600 CPU @3.40 GHz), using four cores in parallel.

### C. Results of the Optimization

Large quantities of individuals evaluations are used to ensure adequate candidate models can be obtained to form the Pareto front of Fig. 12. On the Pareto front, one gets nearly

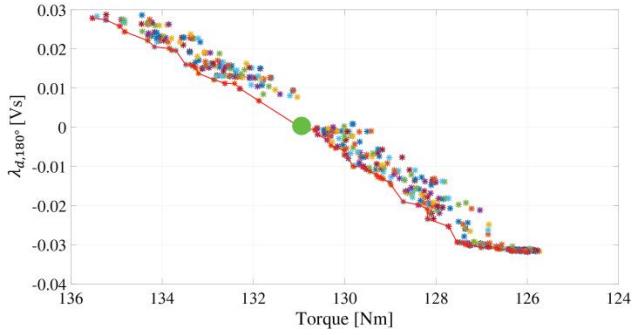


Fig. 12. Pareto front of CW-SPM design optimization

zero  $\lambda_{d,180^\circ}$  is chosen as the final solution (green marker).

#### D. Selection of Number of Turns

The FEA calculated power envelope of design candidate is presented in Fig. 13. The figure shows that changing the number of turns modifies the height of the power plateau and not the nominal torque. From Equation (6),  $k_j$  is proportional the combination of  $(N_s I)$ . As given the key input  $k_j$ ,  $N_s$  is inversely proportional to machine current, which is directly relates to maximum power. In turn,

$$N'_s/N_s = P_{ch}/P_{ch}' \quad (10)$$

Consequently, the number of turns  $N_s$  is adjusted so that the motor current matches the power requirement at maximum speed (10). With constant  $k_j$ , reducing  $N_s$  means increasing the machine current so to keep the product  $N_s I$  constant. Therefore, torque, related to  $N_s I$ , is the same for both cases. The power requirement (50 kW) is met here with  $N_s = 24$  (56 kW), shown in Fig.13.

## VI. NON MAGNETIC ASPECTS

### A. Temperature Estimation

A simplified thermal model integrated into SyR-e estimates the copper temperature given the loading condition  $k_j$  ( $W/m^2$ ). This model is based on radial heat transfer between stator copper and housing. Axial effect is neglected (2D model). Housing temperature is set. The steady-state copper temperature is estimated after the loading factor  $k_j$ , the total stator slot area, slot filling factor and housing temperature [22]. The user can immediately check if the considered  $k_j$  is compatible with the target copper temperature. In this research, the target copper temperature was 130°C and estimated copper temperature for PM-SyRM was 131°C. Finally, copper and magnet temperatures are verified using a lumped parameter transient thermal model available in *Infolytica/Motorsolve* [23], with reference to the selected driving cycle. Made up of 4 ECE and 1 EUDC cycles, the NEDC driving cycle has been repeated six times in two hours through the test, with the coolant temperature at 60°C and flow rate at 10 liter/min. The temperature result for CW-SPM is reported in Fig. 14.

### B. Centrifugal Stress Analysis

Centrifugal stress at maximum speed is evaluated by SyR-e via simplified structural equations for each candidate design.

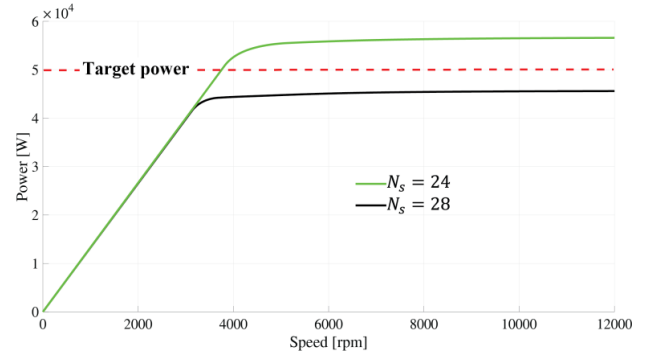


Fig. 13. Power profile of CW-SPM

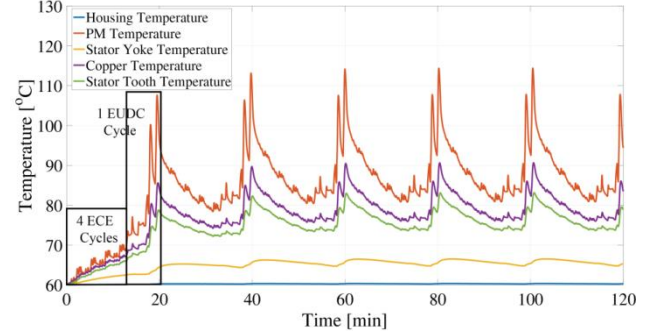


Fig. 14. Temperature result for CW-SPM under repeated NEDC conditions

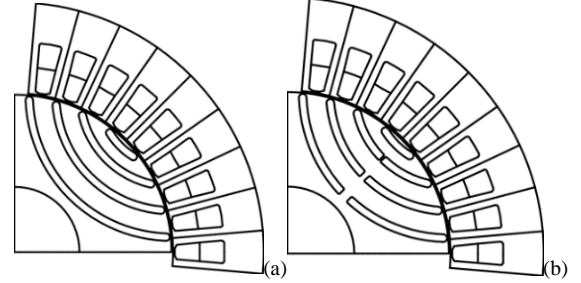


Fig. 15. Automatic design of additional radial bridges for different speed ratings. a) Max speed 3,000 rpm; b) Max speed 12,000 rpm

If needed, additional radial bridges are automatically calculated and included in the barriers of PM-SyRM rotors. The dimensions of the additional radial bridges are evaluated via the simplified structural model described in [24]. The higher the speed rating, the thicker such additional bridges will be, as represented in Fig. 15. Same as for the copper temperature estimation, also stress verification is seamless, in terms of computational time. Off-line validation performed with static 2D finite element analysis (SolidWorks) tells that peak stress in the bridges is 333 MPa at 12,000 rpm. The margin to yield point is 455 MPa, corresponding to a maximum overspeed limit equal to 14,000 rpm with these bridges. Safety factor used in preliminary and end-of-line structural verifications is obtained pursuing 80% of the material's yields strength, thus 20% safety, or 25% overspeed.

## VII. RESULTS

The final structures of both motors are shown in Fig.16. Compared with previous motors [13], the present PM-SyRM has two cavities in each layer, instead of three, making it easier to manufacture. In terms of CW-SPM, the magnets

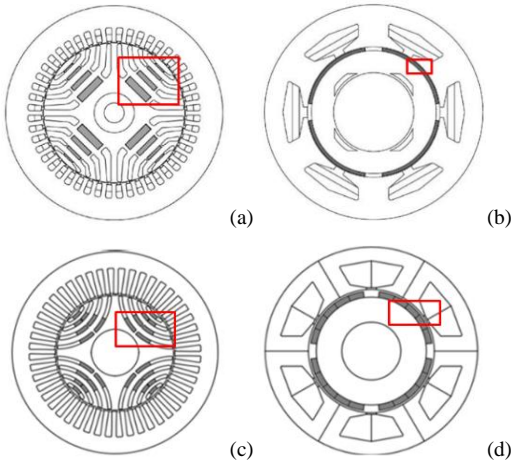


Fig. 16. Motor structures: a) PM-SyRM in [13]; b) CW-SPM in [13]; c) present PM-SyRM; d) present CW-SPM

(grey parts) are both radially and axially segmented into 5 parts, respectively. PMs are thicker than ones in [13] to prevent irreversible demagnetization. Conversely, the cost of magnet is higher.

As mentioned before, the final metric of this study are torque and power curves, as well as efficiency maps. Firstly, flux linkage maps ( $\lambda_d \cdot \lambda_q$ ) of two motors are evaluated off-line via SyR-e over a current domain as large as 360A x 360A in  $i_d, i_q$ . Afterwards, torque maps are calculated by (11):

$$T = \frac{3}{2} \cdot p \cdot (\lambda_d \cdot i_q - \lambda_q \cdot i_d) \quad (11)$$

Based on these maps, the MTPA control law is obtained, valid at low speed. When voltage limit is met, the current vector is further rotated for flux weakening (Fig. 3). Another script available in SyR-e builds the flux weakening control law, including the MTPV trajectory and minimization of total loss for each torque and speed combination.

#### A. Torque and Power Curves

Fig. 17 shows the torque curves of the two machines. Both PM-SyR and CW-SPM machines have a torque at maximum current condition that is markedly higher than the corresponding one in [13], which demonstrates an increase of the transient capability of the powertrain. This is true also at maximum speed, where present motors get higher torque (50 Nm) than those of benchmark motors (39 Nm). Dealing with the power curves of Fig. 18, both motors show similar power curves in characteristic current conditions, having very similar values of  $I_{ch}$ . As expected, the PM-SyRM has better power overload capability, compared with CW-SPM (nearly none, Fig. 18).

#### B. Loss and Efficiency Maps

Power losses of the two motors are FEA evaluated through MagNet/Infolytica, including core, PM, and copper losses. Simulations are repeated over the machine current domain at a single speed value. Then, frequency is adapted to the different speed conditions using the modified Steinmetz approach described in [25], using the coefficients of the magnetic steel in use. Fig. 19 shows the efficiency maps of the two motors.

As expected, the PM-SyRM has a good efficiency all over

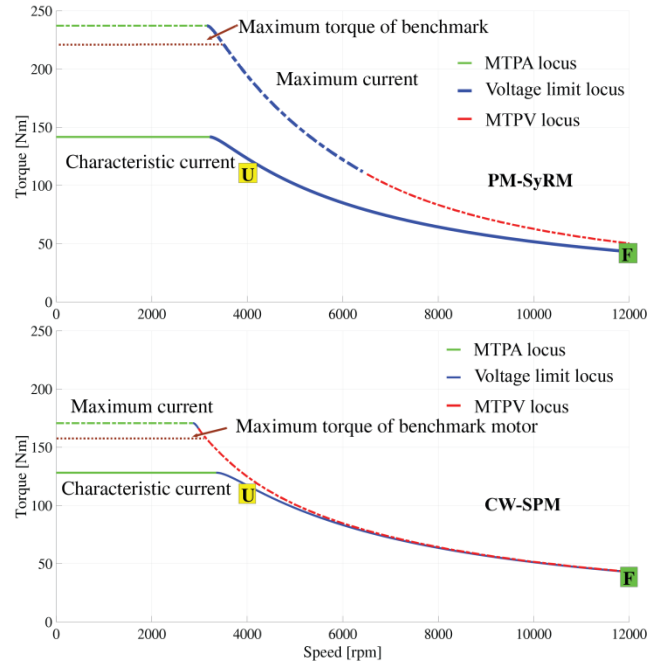


Fig. 17. Torque curves of two motors at their characteristic current and at maximum inverter current, considering the maximum voltage limit

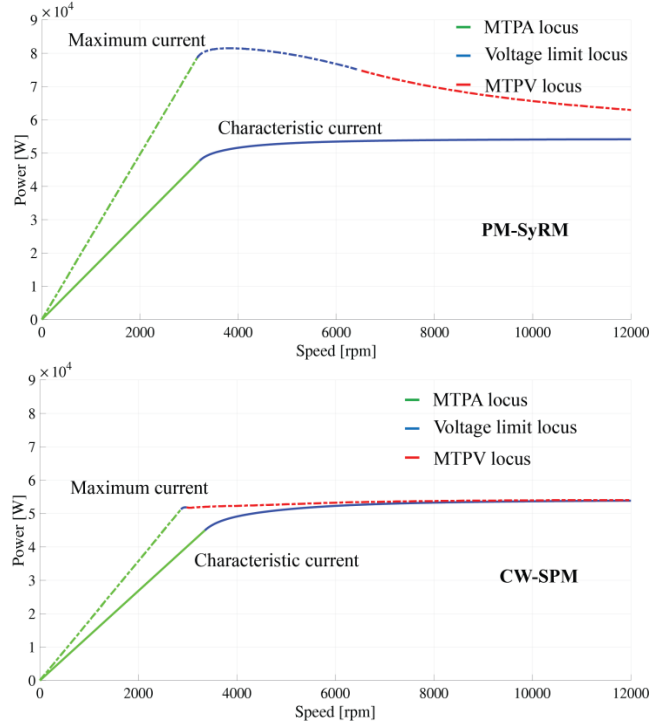


Fig. 18. Power curves of two motors at their characteristic current and at maximum inverter current, considering the maximum voltage limit

the speed domain, including at high speed. Burdened by high PM loss, the high-speed efficiency of CW-SPM is much lower than that of PM-SyRM. Loss details are reported in Fig. 20, for operating points U and F. Compared to the efficiency maps reported in [13], efficiency distributions are similar to the ones of the respective benchmark motor. Both present designs show an increase of peak efficiency (97% versus 96% in both cases). This is related to the better torque per copper loss factor of both new designs, as put in evidence by the loss split

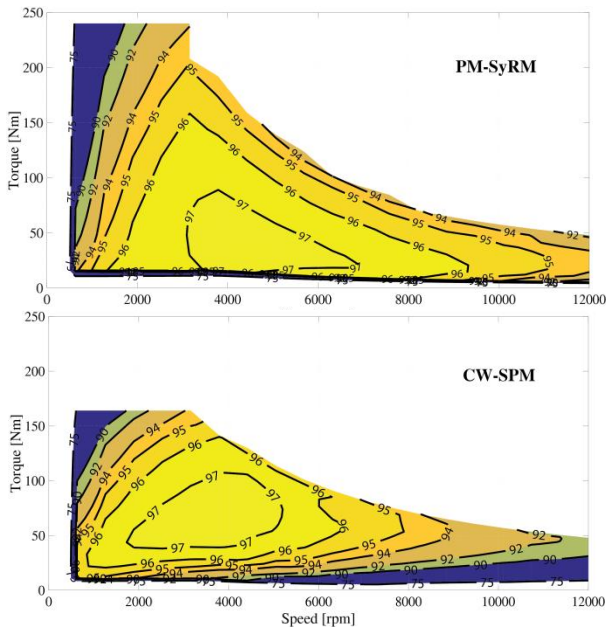


Fig. 19. Efficiency maps of the two machines

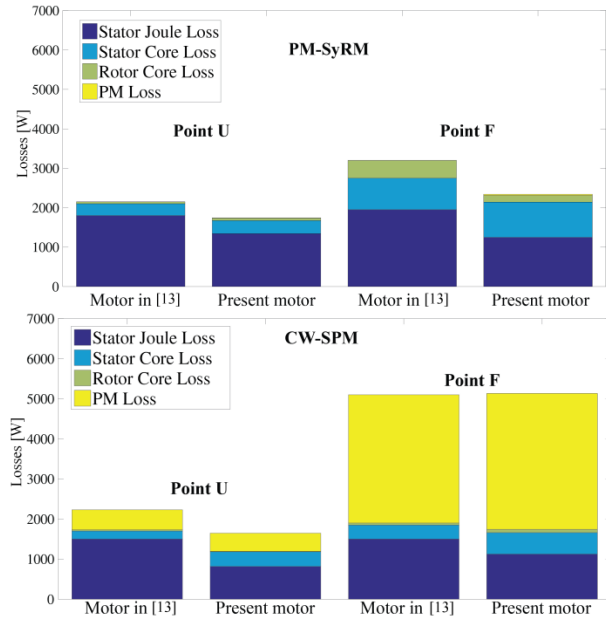


Fig. 20. Power loss at specific points of the new motors, and comparison with the ones in [13]

of Fig. 20.

The magnets of the CW-SPM machine are segmented both axial and radial wise (5 segments per direction) for diminishing eddy current loss. Nevertheless, the motor is still burdened by high magnet loss at high speed (point F). In addition, copper loss grows from point U to point F, due to the significant power loss de-excitation current component. Compared to the benchmark CW-SPM motor, although copper loss is lower for the same operating point, total loss at point F is the same, due to augmented magnet loss. Higher magnet loss come from the larger magnet volume of the new design (+59%, see Table I), mainly related to the augmented airgap (1.0 mm instead of 0.7 mm).

The magnet loss of the PM-SyRM is negligible, as

expected.

## VIII. CONCLUSION

The paper presents two different design approaches for the design of PMSMs for traction. The design tool used in the paper consists of Matlab scripts available online and includes design equations, magnetic FEA, multi objective optimization, simplified structural and thermal co-design. The PM-SyRM design example gave evidence of the parametric design approach, based on design equations and FEA validation. The CW-SPM machine example accounts for automatic design capability of SyR-e, based on MODE optimization. Besides providing comprehensive design procedures for PM-SyR and CW-SPM machines for traction, the paper suggests new design methodologies, such as the goal function  $\lambda_{d,180^\circ}$  that summarizes flux weakening capability in one FEA simulation, or the use of the fictitious magnet and the magnet substitution principles to design the magnets of the PM-SyR machine. Future work will be dedicated to integration of core and PM loss into the SyR-e/FEMM pipeline, and to the improvement of the structural and thermal calculation accuracy.

## REFERENCES

- [1] W. Cao, B. C. Mecrow, G. J. Atkinson, J. W. Bennett and D. J. Atkinson, "Overview of Electric Motor Technologies Used for More Electric Aircraft (MEA)," in *IEEE Transactions on Industrial Electronics*, vol. 59, no. 9, pp. 3523-3531, Sept. 2012.
- [2] A. M. EL-Refaie, "Motors/generators for traction /propulsion applications: A review," *2011 IEEE International Electric Machines & Drives Conference (IEMDC)*, pp. 490-497, 2011.
- [3] Burress, T.; Campbell, S., "Benchmarking EV and HEV power electronics and electric machines," *Transportation Electrification Conference and Expo (ITEC), 2013 IEEE*, pp.1-6, 16-19 June 2013
- [4] S. Li, Y. Li, W. Choi and B. Sarlioglu, "High-Speed Electric Machines: Challenges and Design Considerations," in *IEEE Transactions on Transportation Electrification*, vol. 2, no. 1, pp. 2-13, March 2016.
- [5] "Rotating Electrical Machines—Part 30-1: Efficiency Classes of line operated AC motors" (IE-Code), Ed. 1, IEC 60034-30-1, Dec. 2014.
- [6] S. Ramarathnam, A. K. Mohammed, B. Bilgin, A. Sathyan, H. Dadkhah and A. Emadi, "A Review of Structural and Thermal Analysis of Traction Motors," in *IEEE Transactions on Transportation Electrification*, vol. 1, no. 3, pp. 255-265, Oct. 2015.
- [7] P. Arumugam *et al.*, "High-Speed Solid Rotor Permanent Magnet Machines: Concept and Design," in *IEEE Transactions on Transportation Electrification*, vol. 2, no. 3, pp. 391-400, Sept. 2016.
- [8] A. Rabiei, T. Thiringer, M. Alatalo and E. A. Grunditz, "Improved Maximum-Torque-Per-Ampere Algorithm Accounting for Core Saturation, Cross-Coupling Effect, and Temperature for a PMSM Intended for Vehicular Applications," in *IEEE Transactions on Transportation Electrification*, vol. 2, no. 2, pp. 150-159, June 2016.
- [9] Z. Yang, F. Shang, I. P. Brown and M. Krishnamurthy, "Comparative Study of Interior Permanent Magnet, Induction, and Switched Reluctance Motor Drives for EV and HEV Applications," in *IEEE Transactions on Transportation Electrification*, vol. 1, no. 3, pp. 245-254, Oct. 2015.
- [10] Cupertino F. *et al.*, "Syre - Synchronous Reluctance (machines) - evolution" [Online]. Available: <http://sourceforge.net/projects/syr-e/> [Accessed: 10- Nov- 2015]
- [11] D. Meeker. "Finite Element Method Magnetics (FEMM)". [Online]. Available: <http://femm.foster-miller.net> [Accessed: 10- Nov- 2015]
- [12] Jurkovic, S.; Rahman, K.; Bae, B.; Patel, N.; Savagian, P., "Next generation Chevy Volt electric machines; design, optimization and control for performance and rare-earth mitigation," *Energy Conversion Congress and Exposition (ECCE), 2015 IEEE*, pp.5219-5226, 20-24 Sept. 2015
- [13] G. Pellegrino, A. Vagati, B. Boazzo and P. Guglielmi, "Comparison of induction and PM synchronous motor drives for EV application

including design examples," *IEEE Trans. Ind. Appl.*, vol. 48, no. 2, pp. 2322-2332, Nov. 2012.

- [14] A. Vagati, "Synchronous reluctance drives tutorial." IEEE-IAS Annual Meeting. 1994 (Chapter 3)
- [15] Vagati, A.; Fratta, A.; Franceschini, G.; Rosso, P., "AC motors for high-performance drives: a design-based comparison," in *IEEE Transactions on Industry Applications*, vol.32, no.5, pp.1211-1219, Sep/Oct 1996
- [16] M. van der Geest, H. Polinder, J. A. Ferreira and M. Christmann, "Power Density Limits and Design Trends of High-Speed Permanent Magnet Synchronous Machines," in *IEEE Transactions on Transportation Electrification*, vol. 1, no. 3, pp. 266-276, Oct. 2015.
- [17] Pellegrino, G.; Cupertino, F.; Gerada, C., "Automatic Design of Synchronous Reluctance Motors Focusing on Barrier Shape Optimization," in *Industry Applications, IEEE Transactions on*, vol.51, no.2, pp.1465-1474, March-April 2015
- [18] Magnet by Infolytica. <http://www.infolytica.com/> [Accessed: 20-Dec-2015]
- [19] DieselNet, Emission Test Cycles—Summary of Worldwide Engine and Vehicle Test Cycles. [Online]. Available: [http://www.dieselnet.com/standards/cycles/ece\\_eudc.php](http://www.dieselnet.com/standards/cycles/ece_eudc.php) [Accessed: 20-Dec-2015]
- [20] Burress, T, Campbell, S, "Evaluation of the 2010 Toyota Prius hybrid synergy drive system" Energy Efficiency and Renewable Energy FreedomCAR and Vehicle Technologies Vehicle Systems Team March 2011.
- [21] Pellegrino, G. Cupertino, F. "IPM motor rotor design by means of FEA-based multi-objective optimization", Industrial Electronics (ISIE), 2010 IEEE International Symposium on, pp. 1340-1346, July, 2010
- [22] A. Boglietti, A. Cavagnino, M. Lazzari and M. Pastorelli, "A simplified thermal model for variable-speed self-cooled industrial induction motor," in *IEEE Transactions on Industry Applications*, vol. 39, no. 4, pp. 945-952, July-Aug. 2003.
- [23] MotorSolve by Infolytica. <http://www.infolytica.com/> [Accessed: 20-Dec-2015]
- [24] M. Di Nardo *et al.*, "End barrier shape optimizations and sensitivity analysis of synchronous reluctance machines," *IECON 2015 - 41st Annual Conference of the IEEE Industrial Electronics Society*, Yokohama, 2015, pp. 002914-002919.
- [25] A. Mahmoudi, W. L. Soong, G. Pellegrino, E. Armando, "Efficiency maps of electrical machines," *Energy Conversion Congress and Exposition (ECCE), 2015 IEEE*, pp. 2791-2799, Sept. 2015



design and multi-objective optimization of electrical machines.

**Chao Lu** received the Master degree in electrical engineering in 2014 from Wuhan University of Technology, Wuhan, China. Currently he is working toward the Ph.D. degree in the field of electric motor design from Politecnico di Torino, Turin, Italy. His research interests include open-source development for traction application, especially in parametric



assisted synchronous reluctance machines.

**Simone Ferrari** received the M. Sc. in electrical engineering from Politecnico di Torino, Turin, Italy in 2016, where he is currently working towards his PhD in electrical engineering. His PhD research project deals with the development of multi-physical and open-source design tools for electrical machines, especially for synchronous reluctance and PM-



University, Denmark, in 2002, at the University of Nottingham, UK, in 2010, and at the University of Wisconsin-Madison, USA, in 2013. Dr. Pellegrino is an Associate Editor for the *IEEE Transactions on Industry Applications* and an IEEE Senior Member.

**Gianmario Pellegrino**, PhD, is an Associate Professor of Electrical Machines and Drives at the Politecnico di Torino, Turin, Italy. Dr. Pellegrino is engaged in several research projects with the industry, and has 30 journal papers, one patent and six Best Paper Awards received from IEEE. He was a visiting fellow at Aalborg